Progress In Electromagnetics Research B, Vol. 61, 55–67, 2014

Finite-Difference Frequency-Domain Algorithm for Modeling Electromagnetic Scattering from General Anisotropic Objects

Raymond C. Rumpf*, Cesar R. Garcia, Eric A. Berry, and Jay H. Barton

Abstract—The finite-difference frequency-domain (FDFD) method is a very simple and powerful approach for rigorous analysis of electromagnetic structures. It may be the simplest of all methods to implement and is excellent for field visualization and for developing new ways to model devices. This paper describes a simple method for incorporating anisotropic materials with arbitrary tensors for both permittivity and permeability into the FDFD method. The algorithm is bench marked by comparing transmission and reflection results for an anisotropic guided-mode resonant filter simulated in HFSS and FDFD. The anisotropic FDFD method is then applied to a lens and cloak designed by transformation optics.

1. INTRODUCTION

The finite-difference frequency-domain (FDFD) method is a simple and powerful numerical method for solving Maxwell's equations [1–4]. It is rigorous, excellent for visualizing the fields, and able to model structures with complex geometries. It is accurate, stable, and the sources of error are well understood. Lastly, it lends itself very well to parallel processing on graphical processing units (GPUs) [5, 6]. The method uses central finite-difference approximations to transform Maxwell's equations into a large set of linear algebraic equations that can be written in matrix form as $\mathbf{Ax} = \mathbf{b}$. The field stored in the column vector $\mathbf{x}$ is calculated by solving $\mathbf{x} = \mathbf{A}^{-1}\mathbf{b}$. A complete discussion of the basic FDFD algorithm for ordinary materials can be found in Ref. [7].

This paper outlines how to implement an anisotropic FDFD (AFDFD) method that can handle fully anisotropic materials. An anisotropic medium is one where the permeability and/or permittivity depend on the direction of the electromagnetic fields. Anisotropy provides additional design freedom that can be used to produce a wide array of useful phenomena including surface waves [8], slow waves [9], invisibility and cloaking [10], double refraction, polarization control [11], and more. Further, very often devices composed of metamaterials can be modeled more efficiently using effective medium theory. "Homogeneous" materials with the effective properties of the metamaterials can be meshed more coarsely compared to the volumetrically complex structures of the metamaterial. In this regard, a method capable of modeling devices with arbitrary dielectric and magnetic anisotropy is very useful.

This paper discusses in detail how the three-dimensional (3D) FDFD method described in Ref. [7] can be modified to incorporate anisotropic materials with arbitrary nine-element tensors for both permittivity and permeability. It also discusses some of the subtleties encountered when dealing with tensor quantities like converting them between coordinate systems, rotating them to an arbitrary orientation, combining them with absorbing boundary conditions, and assigning them to points on a grid. Unfortunately, in general anisotropic media Maxwell's equations do not simply for two-dimensional or even one-dimensional analysis due to the complete coupling of the fields. For this reason, it is most straight forward to develop just a 3D FDFD code and use that to model lower dimensional problems. This can be done with virtually no decrease in efficiency if the appropriate precautions are taken. Using

Received 16 July 2014, Accepted 10 September 2014, Scheduled 12 September 2014

* Corresponding author: Raymond C. Rumpf (rcrumpf@utep.edu).

The authors are with the EM Lab, W. M. Keck Center for 3D Innovation, University of Texas at El Paso, USA.

the 3D algorithm this way allows the grid to lie in any plane that is desired. This is advantageous when the algorithm is being used in conjunction with other numerical methods and one is trying to maintain consistent coordinates.

While some papers can be found on FDFD analysis of anisotropic structures [12–18], none of these outline a general purpose method for 3D scattering analysis of devices containing arbitrary permittivity $[\varepsilon]$ and permeability $[\mu]$ tensors. The majority of these papers [12, 14, 15, 18–21] describe waveguide analysis and not scattering. The papers covering scattering [13, 16, 17, 22] are all restricted to two-dimensions and all but Ref. [22] place restrictions on the tensor quantities. This paper describes a general purpose FDFD technique that is rigorous, fully 3D, and incorporates arbitrary material tensors for both permittivity and permeability. The paper is organized as follows. First, the standard formulation of the anisotropic 3D-FDFD method is presented in order to calculate the wave matrix **A**. Second, it is shown how to apply the powerful total-field/scattered-field (TF/SF) technique [22–24] to incorporate sources. Finally, several practical examples are given before the paper is concluded.

2. FORMULATION OF THE METHOD

The formulation and implementation of the basic FDFD method is described in detail in Ref. [7], but only diagonal material tensors $[\mu]$ and $[\varepsilon]$ were considered. The following text outlines how the formulation is generalized to incorporate arbitrary material tensors. After normalizing the magnetic field according to $\vec{\tilde{H}} = -j\eta_0\vec{H}$, Maxwell's curl equations with a uniaxial PML (UPML) [25–27] can be written as

$$\nabla \times \vec{E} = k_0 [\mu_r][s] \vec{\tilde{H}} \tag{1}$$

$$\nabla \times \vec{\tilde{H}} = k_0 [\varepsilon_r][s] \vec{E} \tag{2}$$

For a UPML, the tensor $[s]$ is expressed as

$$[s] = \begin{bmatrix} \frac{s_y s_z}{s_x} & 0 & 0 \\ 0 & \frac{s_x s_z}{s_y} & 0 \\ 0 & 0 & \frac{s_x s_y}{s_z} \end{bmatrix} \tag{3}$$

Without any approximation to the material tensors, Eqs. (1) and (2) can be expanded into the following set of six coupled partial differential equations. The μ'_{ij} and ε'_{ij} terms are relative coefficients because the free space constants μ_0 and ε_0 have been factored out and absorbed into the normalized grid coordinates [7]. In addition, the PML parameters s_x, s_y, and s_z are multiplied into the constitutive parameters such that $[\mu'_r] = [\mu_r][s]$ and $[\varepsilon'_r] = [\varepsilon_r][s]$.

$$\frac{\partial E_z}{\partial \tilde{y}} - \frac{\partial E_y}{\partial \tilde{z}} = \mu'_{xx}\tilde{H}_x + \mu'_{xy}\tilde{H}_y + \mu'_{xz}\tilde{H}_z \tag{4}$$

$$\frac{\partial E_x}{\partial \tilde{z}} - \frac{\partial E_z}{\partial \tilde{x}} = \mu'_{yx}\tilde{H}_x + \mu'_{yy}\tilde{H}_y + \mu'_{yx}\tilde{H}_z \tag{5}$$

$$\frac{\partial E_y}{\partial \tilde{x}} - \frac{\partial E_x}{\partial \tilde{y}} = \mu'_{zx}\tilde{H}_x + \mu'_{zy}\tilde{H}_y + \mu'_{zz}\tilde{H}_z \tag{6}$$

$$\frac{\partial \tilde{H}_z}{\partial \tilde{y}} - \frac{\partial \tilde{H}_y}{\partial \tilde{z}} = \varepsilon'_{xx}E_x + \varepsilon'_{xy}E_y + \varepsilon'_{zx}E_z \tag{7}$$

$$\frac{\partial \tilde{H}_x}{\partial \tilde{z}} - \frac{\partial \tilde{H}_x}{\partial \tilde{x}} = \varepsilon'_{yx}E_x + \varepsilon'_{yy}E_y + \varepsilon'_{yz}E_z \tag{8}$$

$$\frac{\partial \tilde{H}_y}{\partial \tilde{x}} - \frac{\partial \tilde{H}_x}{\partial \tilde{y}} = \varepsilon'_{zx}E_x + \varepsilon'_{zy}E_y + \varepsilon'_{zz}E_z \tag{9}$$

$$[\mu'_r] = \begin{bmatrix} \mu'_{xx} & \mu'_{xy} & \mu'_{xz} \\ \mu'_{yx} & \mu'_{yy} & \mu'_{yz} \\ \mu'_{zx} & \mu'_{zy} & \mu'_{zz} \end{bmatrix} = \begin{bmatrix} \mu_{xx}\frac{s_y s_z}{s_x} & \mu_{xy}\frac{s_x s_z}{s_y} & \mu_{xz}\frac{s_x s_y}{s_z} \\ \mu_{yx}\frac{s_y s_z}{s_x} & \mu_{yy}\frac{s_x s_z}{s_y} & \mu_{yz}\frac{s_x s_y}{s_z} \\ \mu_{zx}\frac{s_y s_z}{s_x} & \mu_{zy}\frac{s_x s_z}{s_y} & \mu_{zz}\frac{s_x s_y}{s_z} \end{bmatrix} \tag{10}$$

$$\left[\varepsilon_r'\right] = \begin{bmatrix} \varepsilon_{xx}' & \varepsilon_{xy}' & \varepsilon_{xz}' \\ \varepsilon_{yx}' & \varepsilon_{yy}' & \varepsilon_{yz}' \\ \varepsilon_{zx}' & \varepsilon_{zy}' & \varepsilon_{zz}' \end{bmatrix} = \begin{bmatrix} \varepsilon_{xx}\frac{s_y s_z}{s_x} & \varepsilon_{xy}\frac{s_x s_z}{s_y} & \varepsilon_{xz}\frac{s_x s_y}{s_z} \\ \varepsilon_{yx}\frac{s_y s_z}{s_x} & \varepsilon_{yy}\frac{s_x s_z}{s_y} & \varepsilon_{yz}\frac{s_x s_y}{s_z} \\ \varepsilon_{zx}\frac{s_y s_z}{s_x} & \varepsilon_{zy}\frac{s_x s_z}{s_y} & \varepsilon_{zz}\frac{s_x s_y}{s_z} \end{bmatrix} \tag{11}$$

Here, the grid coordinates have been normalized according to

$$\tilde{x} = k_0 x \quad \tilde{y} = k_0 y \quad \tilde{z} = k_0 z \tag{12}$$

2.1. Finite-difference Approximation of Maxwell's Equations

Following the procedure outlined in [7], the fields and materials are assigned to discrete points on a Yee grid [28] and the derivatives in Eqs. (4)–(9) are approximated using central finite-differences [29]. The integer variables i, j, and k are array indices.

$$\begin{aligned} &\frac{E_z\big|^{i,j+1,k} - E_z\big|^{i,j,k}}{\Delta\tilde{y}} - \frac{E_y\big|^{i,j,k+1} - E_y\big|^{i,j,k}}{\Delta\tilde{z}} \\ &= \mu_{xx}'\tilde{H}_x\Big|^{i,j,k} + \frac{\mu_{xy}'\tilde{H}_y\Big|^{i-1,j,k} + \mu_{xy}'\tilde{H}_y\Big|^{i,j,k} + \mu_{xy}'\tilde{H}_y\Big|^{i-1,j+1,k} + \mu_{xy}'\tilde{H}_y\Big|^{i,j+1,k}}{4} \\ &\quad + \frac{\mu_{xz}'\tilde{H}_z\Big|^{i-1,j,k} + \mu_{xz}'\tilde{H}_z\Big|^{i,j,k} + \mu_{xz}'\tilde{H}_z\Big|^{i-1,j,k+1} + \mu_{xz}'\tilde{H}_z\Big|^{i,j,k+1}}{4} \end{aligned} \tag{13}$$

$$\begin{aligned} &\frac{E_x\big|^{i,j,k+1} - E_x\big|^{i,j,k}}{\Delta\tilde{z}} - \frac{E_z\big|^{i+1,j,k} - E_z\big|^{i,j,k}}{\Delta\tilde{x}} \\ &= \frac{\mu_{yx}'\tilde{H}_x\Big|^{i,j,k} + \mu_{yx}'\tilde{H}_x\Big|^{i+1,j,k} + \mu_{yx}'\tilde{H}_x\Big|^{i,j-1,k} + \mu_{yx}'\tilde{H}_x\Big|^{i+1,j-1,k}}{4} + \mu_{yy}'\tilde{H}_y\Big|^{i,j,k} \\ &\quad + \frac{\mu_{yz}'\tilde{H}_z\Big|^{i,j-1,k} + \mu_{yz}'\tilde{H}_z\Big|^{i,j,k} + \mu_{yz}'\tilde{H}_z\Big|^{i,j-1,k+1} + \mu_{yz}'\tilde{H}_z\Big|^{i,j,k+1}}{4} \end{aligned} \tag{14}$$

$$\begin{aligned} &\frac{E_y\big|^{i+1,j,k} - E_y\big|^{i,j,k}}{\Delta\tilde{x}} - \frac{E_x\big|^{i,j+1,k} - E_x\big|^{i,j,k}}{\Delta\tilde{y}} \\ &= \frac{\mu_{zx}'\tilde{H}_x\Big|^{i,j,k} + \mu_{zx}'\tilde{H}_x\Big|^{i+1,j,k} + \mu_{zx}'\tilde{H}_x\Big|^{i,j,k-1} + \mu_{zx}'\tilde{H}_x\Big|^{i+1,j,k-1}}{4} \\ &\quad + \frac{\mu_{zy}'\tilde{H}_y\Big|^{i,j,k} + \mu_{zy}'\tilde{H}_y\Big|^{i,j+1,k} + \mu_{zy}'\tilde{H}_y\Big|^{i,j,k-1} + \mu_{zy}'\tilde{H}_y\Big|^{i,j+1,k-1}}{4} + \mu_{zz}'\tilde{H}_z\Big|^{i,j,k} \end{aligned} \tag{15}$$

$$\begin{aligned} &\frac{\tilde{H}_z\Big|^{i,j,k} - \tilde{H}_z\Big|^{i,j-1,k}}{\Delta\tilde{y}} - \frac{\tilde{H}_y\Big|^{i,j,k} - \tilde{H}_y\Big|^{i,j,k-1}}{\Delta\tilde{z}} = \varepsilon_{xx}'E_x\big|^{i,j,k} \\ &\quad + \frac{\varepsilon_{xy}'E_y\big|^{i,j-1,k} + \varepsilon_{xy}'E_y\big|^{i,j,k} + \varepsilon_{xy}'E_y\big|^{i+1,j-1,k} + \varepsilon_{xy}'E_y\big|^{i+1,j,k}}{4} \\ &\quad + \frac{\varepsilon_{xz}'E_z\big|^{i,j,k} + \varepsilon_{xz}'E_z\big|^{i+1,j,k} + \varepsilon_{xz}'E_z\big|^{i,j,k-1} + \varepsilon_{xz}'E_z\big|^{i+1,j,k-1}}{4} \end{aligned} \tag{16}$$

$$\begin{aligned} &\frac{\tilde{H}_x\Big|^{i,j,k} - \tilde{H}_x\Big|^{i,j,k-1}}{\Delta\tilde{z}} - \frac{\tilde{H}_z\Big|^{i,j,k} - \tilde{H}_z\Big|^{i-1,j,k}}{\Delta\tilde{x}} \\ &= \frac{\varepsilon_{yx}'E_x\big|^{i-1,j,k} + \varepsilon_{yx}'E_x\big|^{i,j,k} + \varepsilon_{yx}'E_x\big|^{i-1,j+1,k} + \varepsilon'\,\varepsilon_{yx}E_x\big|^{i,j+1,k}}{4} + \varepsilon_{yy}'E_y\big|^{i,j,k} \end{aligned}$$

$$+\frac{\varepsilon'_{yz}E_z\Big|^{i,j,k}+\varepsilon'_{yz}E_z\Big|^{i,j+1,k}+\varepsilon'_{yz}E_z\Big|^{i,j,k-1}+\varepsilon'_{yz}E_z\Big|^{i,j+1,k-1}}{4} \tag{17}$$
$$\frac{\tilde{H}_y\Big|^{i,j,k}-\tilde{H}_y\Big|^{i-1,j,k}}{\Delta\tilde{x}}-\frac{\tilde{H}_x\Big|^{i,j,k}-\tilde{H}_x\Big|^{i,j-1,k}}{\Delta\tilde{y}}$$

$$=\frac{\varepsilon'_{zx}E_x\Big|^{i-1,j,k}+\varepsilon'_{zx}E_x\Big|^{i,j,k}+\varepsilon'_{zx}E_x\Big|^{i-1,j,k+1}+\varepsilon'_{zx}E_x\Big|^{i,j,k+1}}{4}$$
$$+\frac{\varepsilon'_{zy}E_y\Big|^{i,j-1,k}+\varepsilon'_{zy}E_y\Big|^{i,j,k}+\varepsilon'_{zy}E_y\Big|^{i,j-1,k+1}+\varepsilon'_{zy}E_y\Big|^{i,j,k+1}}{4}+\varepsilon'_{zz}E_z\Big|^{i,j,k} \tag{18}$$

In these equations, the terms containing off diagonal tensor elements require special treatment because each term in a finite-difference equation must exist at the same point in space. In Eq. (13), for example, each term must exist at the same point as $\tilde{H}_x$. The central finite-difference ensures that the derivative terms on the left exist at this point. The last two terms on the right side of this equation are averaged at four points in the grid to interpolate the values at the same point as $\tilde{H}_x$. The same interpolation operation is used on every term in Eqs. (13)–(18) containing an off diagonal tensor element. Figure 1 illustrates the Yee cell and summarizes where each of the tensor elements are defined to exist relative to the field components. The tensor elements μ'_{xx}, μ'_{yx}, and μ'_{zx} are placed on the Yee grid at the same points as $\tilde{H}_x$. The tensor elements μ'_{xy}, μ'_{yy}, and μ'_{zy} are placed at the same points as $\tilde{H}_y$. The tensor elements μ'_{xz}, μ'_{yz}, and μ'_{zz} are placed at the same points as $\tilde{H}_z$. Similarly for the permittivity, the tensor elements ε'_{xx}, ε'_{yx}, and ε'_{zx} are placed on the Yee grid at the same points as E_x. The tensor elements ε'_{xy}, ε'_{yy}, and ε'_{zy} are placed at the same points as E_y. The tensor elements ε'_{xz}, ε'_{yz}, and ε'_{zz} are placed at the same points as E_z.

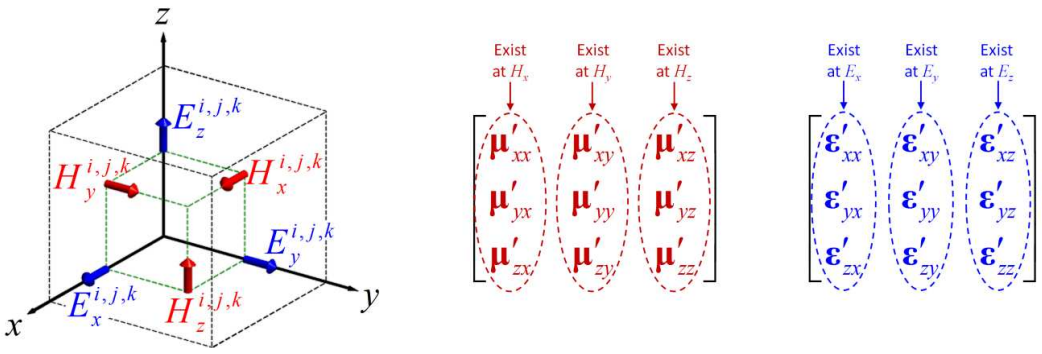

Figure 1. 3D Yee cell along with position of the tensor elements.

2.2. Maxwell's Equations in Matrix Form

Each of Eqs. (13)–(18) is written once for every cell in the grid so each finite-difference equation produces a large set of linear algebraic equations. Each set of equations can be written in matrix form. To do this, interpolation matrices $\mathbf{R}_i^{\pm}$ are introduced to perform the four-point averaging. These will be discussed in more detail later.

$$\mathbf{D}_y^e\mathbf{e}_z-\mathbf{D}_z^e\mathbf{e}_y=\boldsymbol{\mu}'_{xx}\tilde{\mathbf{h}}_x+\mathbf{R}_x^-\mathbf{R}_y^+\boldsymbol{\mu}'_{xy}\tilde{\mathbf{h}}_y+\mathbf{R}_x^-\mathbf{R}_z^+\boldsymbol{\mu}'_{xz}\tilde{\mathbf{h}}_z \tag{19}$$
$$\mathbf{D}_z^e\mathbf{e}_x-\mathbf{D}_x^e\mathbf{e}_z=\mathbf{R}_y^-\mathbf{R}_x^+\boldsymbol{\mu}'_{yx}\tilde{\mathbf{h}}_x+\boldsymbol{\mu}'_{yy}\tilde{\mathbf{h}}_y+\mathbf{R}_y^-\mathbf{R}_z^+\boldsymbol{\mu}'_{yz}\tilde{\mathbf{h}}_z \tag{20}$$
$$\mathbf{D}_x^e\mathbf{e}_y-\mathbf{D}_y^e\mathbf{e}_x=\mathbf{R}_z^-\mathbf{R}_x^+\boldsymbol{\mu}'_{zx}\tilde{\mathbf{h}}_x+\mathbf{R}_z^-\mathbf{R}_y^+\boldsymbol{\mu}'_{zy}\tilde{\mathbf{h}}_y+\boldsymbol{\mu}'_{zz}\tilde{\mathbf{h}}_z \tag{21}$$
$$\mathbf{D}_y^h\tilde{\mathbf{h}}_z-\mathbf{D}_z^h\tilde{\mathbf{h}}_y=\boldsymbol{\varepsilon}'_{xx}\mathbf{e}_x+\mathbf{R}_x^+\mathbf{R}_y^-\boldsymbol{\varepsilon}'_{xy}\mathbf{e}_y+\mathbf{R}_x^+\mathbf{R}_z^-\boldsymbol{\varepsilon}'_{xz}\mathbf{e}_z \tag{22}$$
$$\mathbf{D}_z^h\tilde{\mathbf{h}}_x-\mathbf{D}_x^h\tilde{\mathbf{h}}_z=\mathbf{R}_y^+\mathbf{R}_x^-\boldsymbol{\varepsilon}'_{yx}\mathbf{e}_x+\boldsymbol{\varepsilon}'_{yy}\mathbf{e}_y+\mathbf{R}_y^+\mathbf{R}_z^-\boldsymbol{\varepsilon}'_{yz}\mathbf{e}_z \tag{23}$$

$$\mathbf{D}_x^h\tilde{\mathbf{h}}_y - \mathbf{D}_y^h\tilde{\mathbf{h}}_x = \mathbf{R}_z^+\mathbf{R}_x^-\boldsymbol{\varepsilon}'_{zx}\mathbf{e}_x + \mathbf{R}_z^+\mathbf{R}_y^-\boldsymbol{\varepsilon}'_{zy}\mathbf{e}_y + \boldsymbol{\varepsilon}'_{zz}\mathbf{e}_z \tag{24}$$

The terms $\mathbf{e}_x$, $\mathbf{e}_y$, $\mathbf{e}_z$, $\tilde{\mathbf{h}}_x$, $\tilde{\mathbf{h}}_y$ and $\tilde{\mathbf{h}}_z$ are column vectors that contain all of the field components throughout the entire grid reshaped into linear arrays. The terms $\boldsymbol{\mu}'_{mn}$ and $\boldsymbol{\varepsilon}'_{mn}$ are diagonal matrices containing the relative tensor elements throughout the grid along their diagonals with the PML incorporated. The terms $\mathbf{D}_x^e$, $\mathbf{D}_y^e$ and $\mathbf{D}_z^e$ are banded matrices that calculate first-order spatial derivatives of the electric fields across the grid. Similarly, the terms $\mathbf{D}_x^h$, $\mathbf{D}_y^h$ and $\mathbf{D}_z^h$ calculate first-order spatial derivatives of the magnetic fields across the grid. These are described in more detail in Ref. [7]. When the 3D code is being used to model 2D or 1D systems, the derivatives along the uniform directions take the special forms provided in Eqs. (25)–(27). The wave vector of the source is given by $\vec{k}_{\text{inc}} = k_{x,\text{inc}}\hat{x} + k_{y,\text{inc}}\hat{y} + k_{z,\text{inc}}\hat{z}$ and $\mathbf{I}$ is the identity matrix.

$$\mathbf{D}_x^e = \mathbf{D}_x^h = -j\frac{k_{x,\text{inc}}}{k_0}\mathbf{I} \quad \text{for devices uniform along } x \tag{25}$$

$$\mathbf{D}_y^e = \mathbf{D}_y^h = -j\frac{k_{y,\text{inc}}}{k_0}\mathbf{I} \quad \text{for devices uniform along } y \tag{26}$$

$$\mathbf{D}_z^e = \mathbf{D}_z^h = -j\frac{k_{z,\text{inc}}}{k_0}\mathbf{I} \quad \text{for devices uniform along } z \tag{27}$$

It is possible to "absorb" both the interpolation matrices and PML terms into the permittivity and permeability tensors. When this is done, the tensor elements are written with a double-prime superscript to remind us that the PML and interpolations have been absorbed into them.

$$\left[\boldsymbol{\mu}''_r\right] = \begin{bmatrix} \boldsymbol{\mu}''_{xx} & \boldsymbol{\mu}''_{xy} & \boldsymbol{\mu}''_{xz} \\ \boldsymbol{\mu}''_{yx} & \boldsymbol{\mu}''_{yy} & \boldsymbol{\mu}''_{yz} \\ \boldsymbol{\mu}''_{zx} & \boldsymbol{\mu}''_{zy} & \boldsymbol{\mu}''_{zz} \end{bmatrix} = \begin{bmatrix} \boldsymbol{\mu}'_{xx} & \mathbf{R}_x^-\mathbf{R}_y^+\boldsymbol{\mu}'_{xy} & \mathbf{R}_x^-\mathbf{R}_z^+\boldsymbol{\mu}'_{xz} \\ \mathbf{R}_y^-\mathbf{R}_x^+\boldsymbol{\mu}'_{yx} & \boldsymbol{\mu}'_{yy} & \mathbf{R}_y^-\mathbf{R}_z^+\boldsymbol{\mu}'_{yz} \\ \mathbf{R}_z^-\mathbf{R}_x^+\boldsymbol{\mu}'_{zx} & \mathbf{R}_z^-\mathbf{R}_y^+\boldsymbol{\mu}'_{zy} & \boldsymbol{\mu}'_{zz} \end{bmatrix} \tag{28}$$

$$\left[\boldsymbol{\varepsilon}''_r\right] = \begin{bmatrix} \boldsymbol{\varepsilon}''_{xx} & \boldsymbol{\varepsilon}''_{xy} & \boldsymbol{\varepsilon}''_{xz} \\ \boldsymbol{\varepsilon}''_{yx} & \boldsymbol{\varepsilon}''_{yy} & \boldsymbol{\varepsilon}''_{yz} \\ \boldsymbol{\varepsilon}''_{zx} & \boldsymbol{\varepsilon}''_{zy} & \boldsymbol{\varepsilon}''_{zz} \end{bmatrix} = \begin{bmatrix} \boldsymbol{\varepsilon}'_{xx} & \mathbf{R}_x^+\mathbf{R}_y^-\boldsymbol{\varepsilon}'_{xy} & \mathbf{R}_x^+\mathbf{R}_z^-\boldsymbol{\varepsilon}'_{xz} \\ \mathbf{R}_y^+\mathbf{R}_x^-\boldsymbol{\varepsilon}'_{yx} & \boldsymbol{\varepsilon}'_{yy} & \mathbf{R}_y^+\mathbf{R}_z^-\boldsymbol{\varepsilon}'_{yz} \\ \mathbf{R}_z^+\mathbf{R}_x^-\boldsymbol{\varepsilon}'_{zx} & \mathbf{R}_z^+\mathbf{R}_y^-\boldsymbol{\varepsilon}'_{zy} & \boldsymbol{\varepsilon}'_{zz} \end{bmatrix} \tag{29}$$

The interpolation matrices $\mathbf{R}_i^{\pm}$ are banded matrices that interpolate quantities across the grid [30]. The sign of the superscript indicates whether the interpolation is calculated by averaging a point with the next or previous point on the grid. In this sense, the subscript indicates in which direction the interpolation is happening. The interpolation matrices are very similar in form to the derivative operators and differ only in signs and scaling. It is important to premultiply the tensor elements by the interpolation matrices because it is the εE and μH products that are being interpolated. As a quick example of what the interpolation matrices look like, they were computed for a two-dimensional grid composed of only 4×4 cells. Using Dirichlet boundary conditions, the interpolation matrices $\mathbf{R}_x^+$ and $\mathbf{R}_y^+$ for this simple case are

$$\mathbf{R}_x^+ = \frac{1}{2}\begin{bmatrix} 1 & 1 & & & & & & & & & & & & & & \\ & 1 & 1 & & & & & & & & & & & & & \\ & & 1 & 1 & & & & & & & & & & & & \\ & & & 1 & 0 & & & & & & & & & & & \\ & & & & 1 & 1 & & & & & & & & & & \\ & & & & & 1 & 1 & & & & & & & & & \\ & & & & & & 1 & 1 & & & & & & & & \\ & & & & & & & 1 & 0 & & & & & & & \\ & & & & & & & & 1 & 1 & & & & & & \\ & & & & & & & & & 1 & 1 & & & & & \\ & & & & & & & & & & 1 & 1 & & & & \\ & & & & & & & & & & & 1 & 0 & & & \\ & & & & & & & & & & & & 1 & 1 & & \\ & & & & & & & & & & & & & 1 & 1 & \\ & & & & & & & & & & & & & & 1 & 1 \\ & & & & & & & & & & & & & & & 1 \end{bmatrix} \tag{30}$$

$$\mathbf{R}_y^+ = \frac{1}{2}\begin{bmatrix} 1 & & & 1 & & & & & & & & & & & & \\ & 1 & & & 1 & & & & & & & & & & & \\ & & 1 & & & 1 & & & & & & & & & & \\ & & & 1 & & & 1 & & & & & & & & & \\ & & & & 1 & & & 1 & & & & & & & & \\ & & & & & 1 & & & 1 & & & & & & & \\ & & & & & & 1 & & & 1 & & & & & & \\ & & & & & & & 1 & & & 1 & & & & & \\ & & & & & & & & 1 & & & 1 & & & & \\ & & & & & & & & & 1 & & & 1 & & & \\ & & & & & & & & & & 1 & & & 1 & & \\ & & & & & & & & & & & 1 & & & 1 & \\ & & & & & & & & & & & & 1 & & & \\ & & & & & & & & & & & & & 1 & & \\ & & & & & & & & & & & & & & 1 & \end{bmatrix} \tag{31}$$

For this simple case, the interpolation matrices are composed of two dominant diagonals. Some off diagonal terms can arise when periodic boundaries or other boundary conditions are incorporated. Additional bands will appear when higher-order interpolation is used. The positive and negative interpolation matrices are related through the complex Hermitian operation as $\mathbf{R}_i^+ = \left(\mathbf{R}_i^-\right)^H$. The interpolation matrices can have complex numbers when there are periodic boundary conditions. Using interpolation matrices in this manner allows straightforward implementation of higher-order interpolation schemes without having to modify the rest of the AFDFD code.

Maxwell's curl equations can now be written in block matrix form as

$$\mathbf{C}^e\vec{\mathbf{e}} = \left[\boldsymbol{\mu}_r''\right]\vec{\tilde{\mathbf{h}}} \tag{32}$$

$$\mathbf{C}^h\vec{\tilde{\mathbf{h}}} = \left[\boldsymbol{\varepsilon}_r''\right]\vec{\mathbf{e}} \tag{33}$$

$$\vec{\mathbf{e}} = \begin{bmatrix} \mathbf{e}_x \\ \mathbf{e}_y \\ \mathbf{e}_z \end{bmatrix} \qquad \vec{\tilde{\mathbf{h}}} = \begin{bmatrix} \tilde{\mathbf{h}}_x \\ \tilde{\mathbf{h}}_y \\ \tilde{\mathbf{h}}_z \end{bmatrix} \tag{34}$$

$$\mathbf{C}^e = \begin{bmatrix} \mathbf{0} & -\mathbf{D}_z^e & \mathbf{D}_y^e \\ \mathbf{D}_z^e & \mathbf{0} & -\mathbf{D}_x^e \\ -\mathbf{D}_y^e & \mathbf{D}_x^e & \mathbf{0} \end{bmatrix} \qquad \mathbf{C}^h = \begin{bmatrix} \mathbf{0} & -\mathbf{D}_z^h & \mathbf{D}_y^h \\ \mathbf{D}_z^h & \mathbf{0} & -\mathbf{D}_x^h \\ -\mathbf{D}_y^h & \mathbf{D}_x^h & \mathbf{0} \end{bmatrix} \tag{35}$$

2.3. Matrix Wave Equation

A matrix wave equation can be derived for the electric field by solving Eq. (32) for $\vec{\tilde{\mathbf{h}}}$ and substituting that expression into Eq. (33). A similar matrix wave equation can be derived for the magnetic field by solving Eq. (33) for $\vec{\mathbf{e}}$ and substituting that expression into Eq. (32). It is useful to write the matrix wave equations in terms of a wave matrix $\mathbf{A}$ and the unknown fields, $\vec{\mathbf{e}}$ or $\vec{\tilde{\mathbf{h}}}$.

$$\mathbf{A}_e\vec{\mathbf{e}} = \mathbf{0} \quad \mathbf{A}_e = \mathbf{C}^h\left[\boldsymbol{\mu}_r''\right]^{-1}\mathbf{C}^e - \left[\boldsymbol{\varepsilon}_r''\right] \tag{36}$$

$$\mathbf{A}_h\vec{\tilde{\mathbf{h}}} = \mathbf{0} \quad \mathbf{A}_h = \mathbf{C}^e\left[\boldsymbol{\varepsilon}_r''\right]^{-1}\mathbf{C}^h - \left[\boldsymbol{\mu}_r''\right] \tag{37}$$

These equations cannot yet be solved because a source has not yet been incorporated.

3. ROTATION OF THE TENSORS

The material tensors at each point in the grid can be completely unique so the anisotropy can be varied in any manner across the grid. Physical tensors have only three degrees of freedom, where three numbers represent the material response along the principle axes ($\hat{a}$, $\hat{b}$, and $\hat{c}$) of the anisotropic material. When

the tensors are expressed in this diagonalized system, the three degrees of freedom are explicit. Most often, anisotropic materials are specified in this manner. The convention is to list the constitutive values along the diagonal in order of increasing magnitude.

$$\begin{bmatrix} \varepsilon_a & 0 & 0 \\ 0 & \varepsilon_b & 0 \\ 0 & 0 & \varepsilon_c \end{bmatrix} \text{ and } \begin{bmatrix} \mu_a & 0 & 0 \\ 0 & \mu_b & 0 \\ 0 & 0 & \mu_c \end{bmatrix} \tag{38}$$

To incorporate a tensor into a Cartesian grid, it is first necessary to convert the tensor given along the principle axes $\left[\varepsilon^{\text{abc}}\right]$ to an equivalent tensor in the coordinates of the model $[\varepsilon^{\text{xyz}}]$. In the present work, Cartesian coordinates are used. The transformation is accomplished using Eq. (39) where $\mathbf{P}$ is a rotation matrix.

$$[\varepsilon^{\text{xyz}}] = \mathbf{P}\left[\varepsilon^{\text{abc}}\right]\mathbf{P}^T \tag{39}$$

$$\mathbf{P} = \begin{bmatrix} \hat{x}\bullet\hat{a} & \hat{x}\bullet\hat{b} & \hat{x}\bullet\hat{c} \\ \hat{y}\bullet\hat{a} & \hat{y}\bullet\hat{b} & \hat{y}\bullet\hat{c} \\ \hat{z}\bullet\hat{a} & \hat{z}\bullet\hat{b} & \hat{z}\bullet\hat{c} \end{bmatrix} \tag{40}$$

The Cartesian tensor can be rotated into any arbitrary orientation using rotation matrices [31]. Equation (41) rotates the tensor $[\varepsilon]$ by angle θ about the ith axis. Rotation matrices are both real and unitary so $[P]^T = [P]^{-1}$.

$$\left[\varepsilon^{\text{rot}}\right] = [P_i(\theta)][\varepsilon^{\text{xyz}}][P_i(\theta)]^T \tag{41}$$

Rotation matrices that rotate about the x, y, and z axes by an angle θ are given by Eq. (42), Eq. (43), and Eq. (44) respectively.

$$[P_x(\theta)] = \begin{bmatrix} 1 & 0 & 0 \\ 0 & \cos\theta & -\sin\theta \\ 0 & \sin\theta & \cos\theta \end{bmatrix} \tag{42}$$

$$[P_y(\theta)] = \begin{bmatrix} \cos\theta & 0 & \sin\theta \\ 0 & 1 & 0 \\ -\sin\theta & 0 & \cos\theta \end{bmatrix} \tag{43}$$

$$[P_z(\theta)] = \begin{bmatrix} \cos\theta & -\sin\theta & 0 \\ \sin\theta & \cos\theta & 0 \\ 0 & 0 & 1 \end{bmatrix} \tag{44}$$

Rotation matrices can also be used in any combination. For example, to rotate a tensor by 30° about the z-axis and then 120° about the x-axis, the following sequence of multiplications should be used.

$$\left[\varepsilon^{\text{rot}}\right] = [P_x(120°)][P_z(30°)][\varepsilon^{\text{xyz}}][P_z(30°)]^T[P_x(120°)]^T \tag{45}$$

4. TOTAL-FIELD/SCATTERED-FIELD FORMULATION

The powerful total-field/scattered-field (TF/SF) technique described in Ref. [7] for incorporating a source can still be applied, but three field components are needed to describe the source. The source field $\vec{\mathbf{e}}_{\text{src}}$ is constructed according to Eq. (46). It is a column vector composed of three smaller column vectors $\mathbf{e}_{x,\text{src}}$, $\mathbf{e}_{y,\text{src}}$, and $\mathbf{e}_{z,\text{src}}$ that each contain the different field components of the source throughout the Yee grid, but reshaped into 1D arrays.

$$\vec{\mathbf{e}}_{\text{src}} = \begin{bmatrix} \mathbf{e}_{x,\text{src}} \\ \mathbf{e}_{y,\text{src}} \\ \mathbf{e}_{z,\text{src}} \end{bmatrix} \tag{46}$$

$$\mathbf{e}_{x,\text{src}} = \begin{bmatrix} e_{x,\text{src}}^{(1,1,1)} \\ e_{x,\text{src}}^{(1,1,2)} \\ \vdots \\ e_{x,\text{src}}^{(N_x,N_y,N_z)} \end{bmatrix} \mathbf{e}_{y,\text{src}} = \begin{bmatrix} e_{y,\text{src}}^{(1,1,1)} \\ e_{y,\text{src}}^{(1,1,2)} \\ \vdots \\ e_{y,\text{src}}^{(N_x,N_y,N_z)} \end{bmatrix} \mathbf{e}_{z,\text{src}} = \begin{bmatrix} e_{z,\text{src}}^{(1,1,1)} \\ e_{z,\text{src}}^{(1,1,2)} \\ \vdots \\ e_{z,\text{src}}^{(N_x,N_y,N_z)} \end{bmatrix} \tag{47}$$

The masking matrix $\mathbf{Q}$ presented in Ref. [7] must be slightly modified and is constructed in the form of Eq. (48). It is a block diagonal matrix composed of three matrices along its diagonal. $\mathbf{Q}_x$ is the scattered-field masking matrix for the E_x field, $\mathbf{Q}_y$ is the scattered-field masking matrix for the E_y field, and $\mathbf{Q}_z$ is the scattered-field masking matrix for the E_z field.

$$\mathbf{Q} = \begin{bmatrix} \mathbf{Q}_x & \mathbf{0} & \mathbf{0} \\ \mathbf{0} & \mathbf{Q}_y & \mathbf{0} \\ \mathbf{0} & \mathbf{0} & \mathbf{Q}_z \end{bmatrix} \tag{48}$$

Given the wave matrix $\mathbf{A}$, source field $\mathbf{f}_{\text{src}}$, and the masking matrix $\mathbf{Q}$, the source vector $\mathbf{b}$ is calculated according to the equation presented in Ref. [7].

$$\mathbf{b} = (\mathbf{QA} - \mathbf{AQ})\,\vec{\mathbf{e}}_{\text{src}} \tag{49}$$

Now that a source has been incorporated, the field is calculated according to Eq. (50). Note that the solution $\vec{\mathbf{e}}$ must be parsed to extract the individual field components $\mathbf{e}_x$, $\mathbf{e}_y$, and $\mathbf{e}_z$. These three terms can then then be reshaped from column vectors back to the original grid.

$$\vec{\mathbf{e}} = \begin{bmatrix} \mathbf{e}_x \\ \mathbf{e}_y \\ \mathbf{e}_z \end{bmatrix} = \mathbf{A}^{-1}\mathbf{b} \tag{50}$$

If needed, the magnetic field can be calculated from the electric field using Eq. (32). This is

$$\vec{\mathbf{h}} = \left[\boldsymbol{\mu}_r''\right]^{-1} \mathbf{C}^e \vec{e} \tag{51}$$

5. BENCHMARK SIMULATIONS

5.1. Scattering from an Anisotropic Guided-Mode Resonance Filter

Guided-mode resonance (GMR) filters consist of two electromagnetically coupled devices; a grating and a slab waveguide [32]. When an external electromagnetic wave is incident on the device and a precise phase matching condition is met, the external wave is diffracted by the grating and coupled into a guided mode within the slab. Due to reciprocity, the guided waves slowly leak back out of the slab waveguide. The leaked wave interferes with the incident wave to produce the overall frequency response.

GMR devices using ruled gratings are inherently sensitive to polarization due to the birefringence imposed by the grating [32–36]. By incorporating anisotropy into the design, it becomes possible to introduce birefringence that counteracts the grating to realize polarization independent designs. Using the AFDFD code, an anisotropic ruled-grating GMR filter was designed to be polarization insensitive. The results were verified by simulating the same design with Ansys HFSS. Both HFSS and AFDFD used a plane wave as a source and periodic boundaries on the sides. AFDFD used UPML's on the top and bottom, but HFSS used Floquet ports.

Figure 2 depicts the spectral response of the anisotropic GMR filter obtained using both HFSS and AFDFD and the results matched almost exactly. Both the transvers electric (TE) and transvers magnetic (TM) modes were made resonant at 24.94 GHz by adjusting the anisotropy of the material. The TE mode exhibited a 0.2% fractional bandwidth while the TM mode exhibited 0.16% fractional bandwidth. Using the method presented in reference [37], a concept of how this device could be realized is illustrated in Figure 3. In this diagram, anisotropy is introduced artificially using an array of air holes formed through the otherwise ordinary dielectric. The array must be highly subwavelength to ensure that it is not resonant.

5.2. Scattering from a Flat Lens for Far-Zone Focusing

Transformation optics (TO) uses coordinate transforms to design electromagnetic devices that can control electromagnetic fields almost arbitrarily [38–40]. Since Maxwell's equations are form invariant [41, 42] the transform can be pulled out of the coordinates and absorbed into the constitutive parameters. When this is done, the electromagnetic fields in the new constitutive parameters behave the same as they did in the transformed coordinate system. Using TO, a flat lens for far-zone focusing was

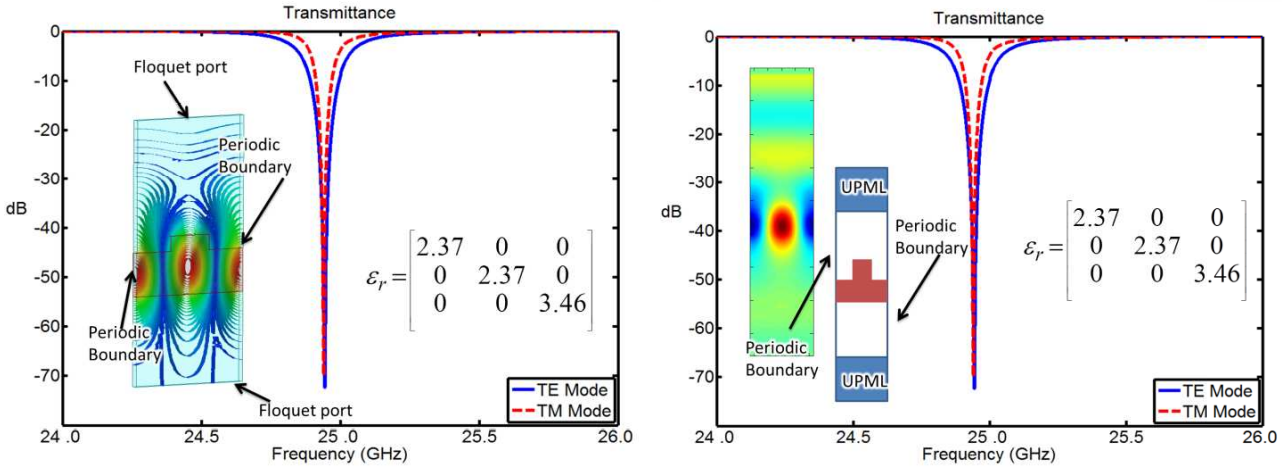

Figure 2. (a) Anisotropic GMR filter spectral response simulated with Ansys HFSS. (b) Anisotropic GMR spectral response simulated with AFDFD.

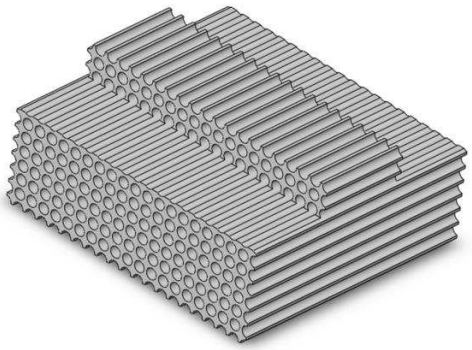

Figure 3. Concept drawing of a GMR filter incorporating artificial anisotropy produced by a highly subwavelength array of holes in the dielectric.

designed in Ref. [43]. The lens effectively converts cylindrical waves into plane waves. In this design, the permittivity and permeability were set equal. The resulting permittivity was

$$\varepsilon'_{xx} = \frac{\sqrt{a^2 - x^2} - g}{l} \tag{52}$$

$$\varepsilon'_{xy} = \varepsilon'_{yx} = \frac{x\,(y-g)}{l\sqrt{a^2 - x^2}} \tag{53}$$

$$\varepsilon'_{yy} = \frac{1}{\sqrt{a^2 - x^2} - g}\left[\frac{x^2\,(y-g)^2}{l\,(a^2 - x^2)} + l\right] \tag{54}$$

$$\varepsilon'_{zz} = \frac{\sqrt{a^2 - x^2} - g}{l} \tag{55}$$

$$\varepsilon'_{zx} = \varepsilon'_{xz} = \varepsilon'_{zy} = \varepsilon'_{yz} = 0 \tag{56}$$

$$a = \left(g^2 + w^2\right)^{1/2} \tag{57}$$

The dimensions in this design were $w = 0.4\,\mathrm{m}$, $g = 0.05\,\mathrm{m}$, and $l = 0.1\,\mathrm{m}$. The material parameters are plotted across a 2D grid in Figure 4.

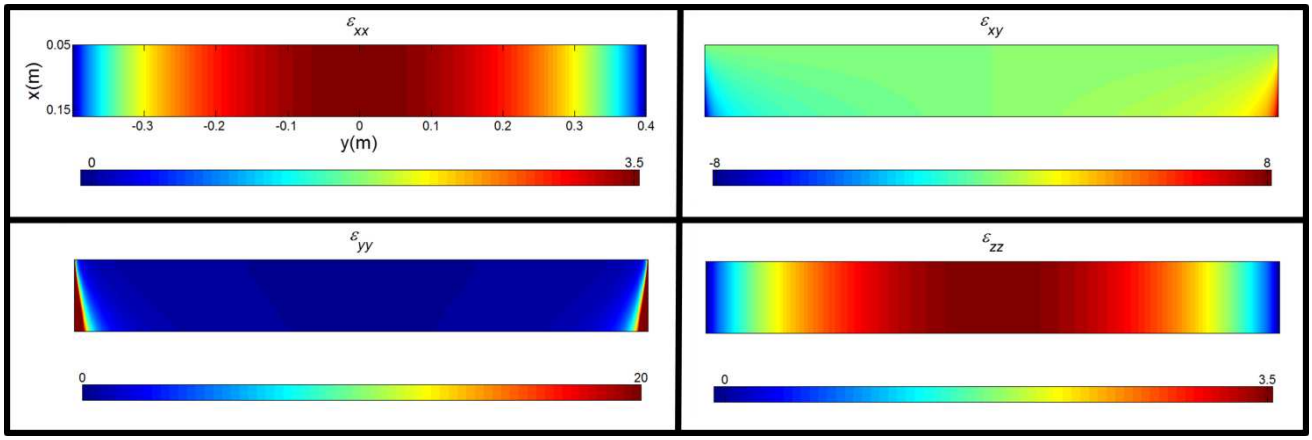

Figure 4. Material parameters for a far-zone lens.

The far zone lens was simulated using the AFDFD method presented here. The field calculated from the simulation is shown in Figure 5. There are UPML's on all four sides of the simulation space. The simulated results are extremely close to those shown in Figure 6 of Ref. [41]. There are slight reflections at the interface of the lens and the cylindrical wave because the materials properties were truncated to eliminate extreme values. Duplicating these results confirms the accuracy of the simple AFDFD method.

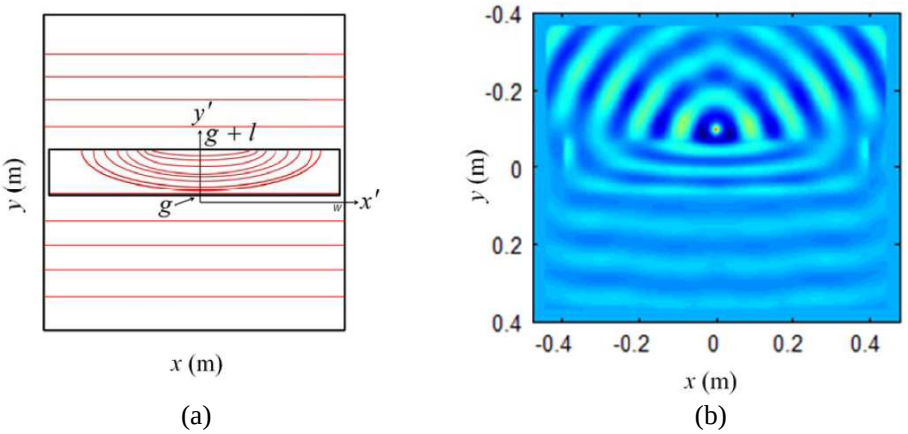

Figure 5. (a) Geometry of coordinate transformation. (b) Simulated far zone lens with AFDFD.

5.3. Scattering from a Cloak

Using TO, cloaks have been designed to work in the microwave region [10] and in the optical region [44]. Using the coordinate transform developed in Ref. [10], a cloak was made using the following coordinate transform in the cylindrical coordinate system. In these equations, the parameter a is the inner radius of the cloak and parameter b is the outer radius.

$$r' = \frac{b-a}{b} r + a \tag{58}$$

$$\theta' = \theta \tag{59}$$

$$z' = z \tag{60}$$

The dimensions used were $a = 10\,\text{cm}$ and $b = 45\,\text{cm}$. For illustration purposes, Eqs. (58)–(60) were converted into Cartesian space and plotted in Figure 6.

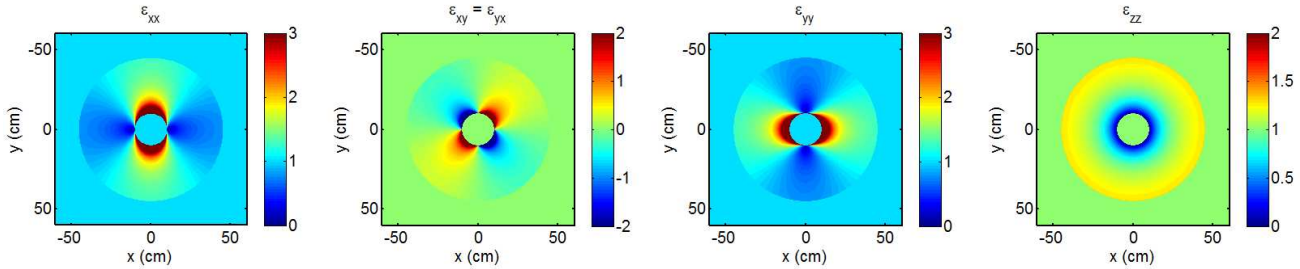

Figure 6. Material parameters of cloak.

The tensor elements not shown in Figure 6 were set to zero. A standard plane wave was simulated using AFDFD with UMPL's on the left and right and Dirichlet boundaries on the other sides. The same plane wave was simulated but with the cloak placed in the center of the simulation space. It can be seen in Figure 7 that the cloak was successfully simulated using AFDFD. The cloak was able to reconstruct a plane wave on the transmitted side of the device.

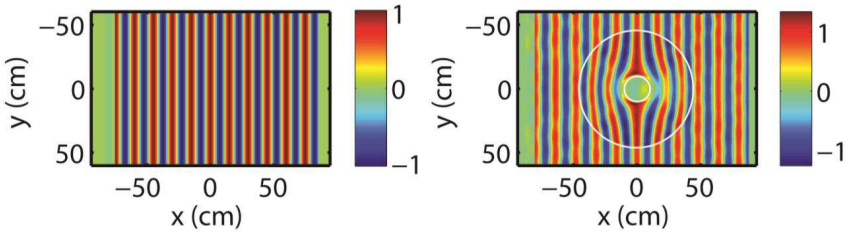

Figure 7. AFDFD simulation of cloak.

6. CONCLUSIONS

It was shown in detail how to modify the 3D FDFD method to be able to incorporate anisotropic materials with arbitrary tensors. It was also shown how to use the 3D code as a 2D code and a 1D code by special treatment of the derivative operators. The method was then successfully benchmarked by simulating an anisotropic GMR filter in HFSS and in AFDFD. Finally, AFDFD was used to simulate a far zone lens and a cloak generated with TO. All of the results obtained using AFDFD matched very closely to results obtained by other tools and other authors.

REFERENCES

1. Luo, G. Q., W. Hong, Z.-C. Hao, B. Liu, W. D. Li, J. X. Chen, et al., "Theory and experiment of novel frequency selective surface based on substrate integrated waveguide technology," *IEEE Transactions on Antennas and Propagation*, Vol. 53, 4035–4043, 2005.
2. Rumpf, R. C., "Design and optimization of nano-optical elements by coupling fabrication to optical behavior," University of Central Florida Orlando, Florida, 2006.
3. Sun, W., K. Liu, and C. A. Balanis, "Analysis of singly and doubly periodic absorbers by frequency-domain finite-difference method," *IEEE Transactions on Antennas and Propagation*, Vol. 44, 798–805, 1996.
4. Wu, S.-D. and E. N. Glytsis, "Volume holographic grating couplers: Rigorous analysis by use of the finite-difference frequency-domain method," *Applied Optics*, Vol. 43, 1009–1023, 2004.
5. Shin, W. and S. Fan, "Choice of the perfectly matched layer boundary condition for frequency-domain Maxwell's equations solvers," *Journal of Computational Physics*, Vol. 231, 3406–3431, 2012.

6. Shin, W. and S. Fan, "Accelerated solution of the frequency-domain Maxwell's equations by engineering the eigenvalue distribution of the operator," *Optics Express*, Vol. 21, 22578–22595, 2013.
7. Rumpf, R. C., "Simple implementation of arbitrarily shaped total-field/scattered-field regions in finite-difference frequency-domain," *Progress In Electromagnetics Research B*, Vol. 36, 221–248, 2012.
8. Takayama, O., L.-C. Crasovan, S. K. Johansen, D. Mihalache, D. Artigas, and L. Torner, "Dyakonov surface waves: A review," *Electromagnetics*, Vol. 28, 126–145, 2008.
9. Figotin, A. and I. Vitebskiy, "Slow-wave resonance in periodic stacks of anisotropic layers," *Physical Review A*, Vol. 76, 053839, 2007.
10. Schurig, D., J. Mock, B. Justice, S. A. Cummer, J. Pendry, A. Starr, et al., "Metamaterial electromagnetic cloak at microwave frequencies," *Science*, Vol. 314, 977–980, 2006.
11. Kwon, D.-H. and D. H. Werner, "Polarization splitter and polarization rotator designs based on transformation optics," *Optics Express*, Vol. 16, 18731–18738, 2008.
12. Al-Barqawi, H., N. Dib, and M. Khodier, "A two-dimensional full-wave finite-difference frequency-domain analysis of ferrite loaded structures," *International Journal of Infrared and Millimeter Waves*, Vol. 29, 443–456, 2008.
13. Loke, V. L., T. A. Nieminen, S. J. Parkin, N. R. Heckenberg, and H. Rubinsztein-Dunlop, "FDFD/T-matrix hybrid method," *Journal of Quantitative Spectroscopy and Radiative Transfer*, Vol. 106, 274–284, 2007.
14. Mielewski, J., A. Cwikla, and M. Mrozowski, "Analysis of shielded anisotropic dielectric resonators using FDFD and the Arnoldi method," *12th International Conference on Microwaves and Radar, MIKON'98*, 335–339, 1998.
15. Pinheiro, H. F., A. J. Giarola, and C. L. D. S. S. Sobrinho, "Dispersion characteristics of asymmetric coupled anisotropic dielectric waveguides using FDFD," *International Journal of Infrared and Millimeter Waves*, Vol. 16, 1965–1975, 1995.
16. Rappaport, C. M. and B. J. McCartin, "FDFD analysis of electromagnetic scattering in anisotropic media using unconstrained triangular meshes," *IEEE Transactions on Antennas and Propagation*, Vol. 39, 345–349, 1991.
17. Rappaport, C. M. and E. Smith, "Anisotropic FDFD computed on conformal meshes," *IEEE Transactions on Magnetics*, Vol. 27, 3848–3851, 1991.
18. Zhao, Y.-J., K.-L. Wu, and K.-K. Cheng, "A compact 2-D full-wave finite-difference frequency-domain method for general guided wave structures," *IEEE Transactions on Microwave Theory and Techniques*, Vol. 50, 1844–1848, 2002.
19. Chen, M.-Y., S.-M. Hsu, and H.-C. Chang, "A finite-difference frequency-domain method for full-vectroial mode solutions of anisotropic optical waveguides with arbitrary permittivity tensor," *Optics Express*, Vol. 17, 5965–5979, 2009.
20. Lavranos, C., G. Kyriacou, and J. Sahalos, "A 2-D finite difference frequency domain (FDFD) eigenvalue method for orthogonal curvilinear coordinates," *PIERS Proceedings*, 397–400, PISA, Italy, Mar. 28–31, 2004.
21. Pereda, J. A., A. Vegas, and A. Prieto, "An improved compact 2D full-wave FDFD method for general guided wave structures," *Microwave and Optical Technology Letters*, Vol. 38, 331–335, 2003.
22. Zainud-Deen, S. H., A. Z. Botros, and M. S. Ibrahim, "Scattering from bodies coated with metamaterial using FDFD method," *Progress In Electromagnetics Research B*, Vol. 2, 279–290, 2008.
23. Taflove, A. and S. C. Hagness, *Computational Electrodynamics*, Vol. 160, Artech House Boston, 2000.
24. Umashankar, K. and A. Taflove, "A novel method to analyze electromagnetic scattering of complex objects," *IEEE Transactions on Electromagnetic Compatibility*, 397–405, 1982.
25. Berenger, J.-P., "A perfectly matched layer for the absorption of electromagnetic waves," *Journal of Computational Physics*, Vol. 114, 185–200, 1994.

26. Margengo, E., C. M. Rappaport, and E. L. Miller, "Optimum PML ABC conductivity profile in FDFD," *IEEE Transactions on Magnetics*, Vol. 35, 1506–1509, 1999.
27. Sacks, Z. S., D. M. Kingsland, R. Lee, and J.-F. Lee, "A perfectly matched anisotropic absorber for use as an absorbing boundary condition," *IEEE Transactions on Antennas and Propagation*, Vol. 43, 1460–1463, 1995.
28. Yee, K. S., "Numerical solution of initial boundary value problems involving Maxwell's equations," *IEEE Transactions on Antennas and Propagation*, Vol. 14, 302–307, 1966.
29. Jordán, K., *Calculus of Finite Differences*, American Mathematical Soc., 1965.
30. Rumpf, R. C., C. R. Garcia, H. H. Tsang, J. E. Padilla, and M. D. Irwin, "Electromagnetic isolation of a microstrip by embedding in a spatially variant anisotropic metamaterial," *Progress In Electromagnetics Research*, Vol. 142, 243–260, 2013.
31. Horn, A., "Doubly stochastic matrices and the diagonal of a rotation matrix," *Amer. J. Math*, Vol. 76, 620–630, 1954.
32. Magnusson, R. and S. Wang, "New principle for optical filters," *Applied Physics Letters*, Vol. 61, 1022–1024, 1992.
33. Barton, J. H., R. C. Rumpf, R. W. Smith, C. L. Kozikowski, and P. A. Zellner, "All-dielectric frequency selective surfaces with few number of periods," *Progress In Electromagnetics Research B*, Vol. 41, 269–283, 2012.
34. Boonruang, S., A. Greenwell, and M. Moharam, "Multiline two-dimensional guided-mode resonant filters," *Applied Optics*, Vol. 45, 5740–5747, 2006.
35. Pung, A. J., S. R. Carl, I. R. Srimathi, and E. G. Johnson, "Method of fabrication for encapsulated polarizing resonant gratings," *IEEE Photonics Technology Letters*, Vol. 25, 1432–1434, 2013.
36. Tibuleac, S. and R. Magnusson, "Reflection and transmission guided-mode resonance filters," *JOSA A*, Vol. 14, 1617–1626, 1997.
37. Garcia, C. R., J. Correa, D. Espalin, J. H. Barton, R. C. Rumpf, R. Wicker, and V. Gonzalez, "3D printing of anisotropic metamaterials," *Progress In Electromagnetics Research Letters*, Vol. 34, 75–82, 2012.
38. Leonhardt, U., "Optical conformal mapping," *Science*, Vol. 312, 1777–1780, 2006.
39. Pendry, J. B., D. Schurig, and D. R. Smith, "Controlling electromagnetic fields," *Science*, Vol. 312, 1780–1782, 2006.
40. Ward, A. and J. Pendry, "Refraction and geometry in Maxwell's equations," *Journal of Modern Optics*, Vol. 43, 773–793, 1996.
41. Landau, L. D. and E. M. Lifshits, *The Classical Theory of Fields*, Vol. 2, Butterworth-Heinemann, 1975.
42. Post, E. J., *Formal Structure of Electromagnetics: General Covariance and Electromagnetics*, Courier Dover Publications, 1997.
43. Kwon, D.-H. and D. H. Werner, "Transformation optical designs for wave collimators, flat lenses and right-angle bends," *New Journal of Physics*, Vol. 10, 115023, 2008.
44. Cai, W., U. K. Chettiar, A. V. Kildishev, and V. M. Shalaev, "Optical cloaking with metamaterials," *Nature Photonics*, Vol. 1, 224–227, 2007.